Numerical Simulation of the Somali Jet

T. N. KRISHNAMURTI, JOHN MOLINARI AND HUA LU PAN

Department of Meteorology, Florida State University, Tallahassee 32306

(Manuscript received 8 March 1976, in revised form 18 August 1976)

ABSTRACT

In this study we show that many of the observed features of the cross-equatorial low-level jet of the Arabian Sea, Indian Ocean and Somalia can be numerically simulated by including 1) the east African and Madagascar mountains, 2) the beta effect and 3) a lateral forcing from the east around 75°E. This lateral forcing at 75°E is, in fact, a solution of another numerical model—one where the land-ocean contrast heating in the meridional direction is incorporated in much detail to simulate the zonally symmetric monsoons, essentially following Murakami *et al.* (1970). This zonally symmetric solution of a very long-term numerical integration from a state of rest exhibits many of the observed characteristics of the broad-scale monsoons at 75°E. This later solution is used as a lateral forcing for the low-level jet simulations over the Arabian Sea–Indian Ocean.

The numerical model presented here is a one-level primitive equation model with a detailed bottom topography and a one-degree latitude grid size.

Results of several controlled numerical experiments suppressing or including orography, the beta effect and the broad-scale lateral monsoon forcing at 75°E are discussed in this paper. When all the three above-mentioned parameters are included, features such as strong winds just downstream from the Madagascar mountains, an equatorial relative speed minimum, an intense jet off the Somali coast and a split of the jet over the northern Arabian Sea are simulated from an initial state of rest. The Ethiopian highland appears crucial for the simulation of the Somali coast strong winds; the Madagascar mountains are most important for the strong winds just downstream from Madagascar. The split in the jet over the Arabian Sea is analyzed as a barotropic instability problem. The beta effect is essential for the simulation of the observed geometry. Experiments with a weak broad-scale monsoon forcing at 75°E fail to produce strong winds over east Africa. The implications of this forcing are analyzed in this paper and some relevant observations are presented.

1. Introduction

Much of our present knowledge of the observational aspects is based on the studies of Bunker (1965) and Findlater (1969a, b, 1971). In this paper we shall use the "Somali jet" in a much broader context. This includes the entire low-level jet and associated flows in a wide domain (Fig. 1).

This diagram is from Findlater's well-known work. It shows the monthly mean airflow at the 1.0 km level for August. Weather stations for which wind observations were available (and from which this analysis is constructed) are shown by arrows and numbers, the numbers indicating wind speed in knots. The salient features of the low-level flows are

1) A wind maximum near the northern tip of Madagascar.

2) A strong wind maximum just downstream from the Somali coast.

3) A major cross-equatorial current from the southern Indian Ocean to the central Arabian Sea.

4) A relative minimum in speed along the axis of strong winds near the equator.

5) A split in the axis of the jet in the Arabian Sea, the more northern branch intersecting the west coast of India near 17°N, while the southerly branch of the split moves eastward just south of India.

The maximum speed on the monthly mean fields is of the order of 18 m s^{-1}. It should, however, be noted that daily wind speeds of the order of 50 m s^{-1} have been reported by Findlater (1969a). Furthermore, it may be noted that the low-level jet penetrates inland over east Africa, however, remaining just to the east of the east African highlands.

In order to illustrate this feature we also present (Fig. 2), a vertical cross section of the meridional wind for an equatorial-zonal plane for several months (Findlater, 1971). This section illustrates the cross-equatorial jet and its proximity to the mountains. The Kenya highlands appear to be a western boundary for this major air current near the equator. This major low-level air current is known to have a maximum wind speed near the 1.5 km level. The gradual formation of this jet may be visualized from Findlater's analysis (Fig. 3). In February a clockwise gyre of air may be

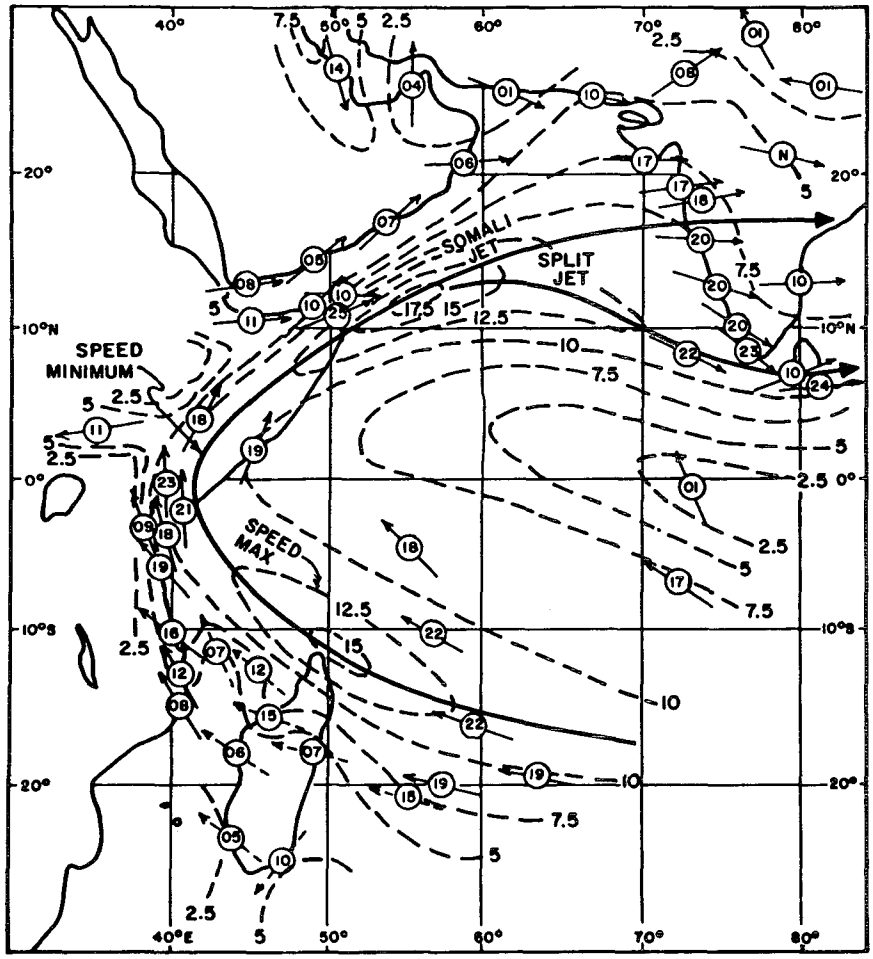

FIG. 1. Findlater's (1971) analysis of 1 km streamlines (solid lines) and isotachs (dashed lines, m s^{-1}) for August. The dark heavy line illustrates the axis of the low-level jet. The locations of observational sites are shown by circles. The enclosed numbers within the circle are the observed monthly mean speed in knots.

seen 10° south of the equator. The circulation progresses northwestward until June, then is relatively steady in position until September. A split in the axis of the jet occurs during the summer months. With the progress of the winter monsoons, the gyre proceeds southeastward to the southern Indian Ocean.

We shall not discuss the observational aspects of transients in this paper. Some discussion of this problem appears in studies by Findlater (1969a), and by Krishnamurti and Bhalme (1976). We feel that the scope of the present simulation study is not relevant for the problem of transients. We shall be primarily concerned with the problem of the numerical simulation and analysis of the five major features listed above.

2. A hypothesis on the formation of the "Somali jet"

Based on the observations of monsoon flows and the present state of our understanding of the general circulation of the monsoon belt, we propose that the following are of importance for the formation of the low-level jet:

1) The differential land–ocean contrast heating over the eastern part of the domain. An example of this thermal forcing was discussed by Murakami *et al.* (1970), and was shown to be of major importance for the dynamics of the broad-scale monsoons.

2) The east African highlands, encompassing the Madagascar mountains as well as the ranges from Kenya to Ethiopia, are important for providing a western boundary intensification of this wind system. There is some similarity in the work we present here and the mechanisms discussed by Lighthill (1969), who has described the Somali Current in the ocean as a western boundary phenomenon.

3) The beta effect.

Our hypothesis is that a simple model incorporating the effects of the above three parameters can simulate

many of the observed features of the cross-equatorial low-level jet. Presently, we do not consider parameters such as local coastal upwelling, air-sea interactions, detailed boundary layer dynamics, detailed vertical resolution, or middle latitude interactions. These may be essential for describing the transients of the problem. However, we feel that the broadscale features of the low-level jet can be described by a simple prescription of the three parameters mentioned above.

In order to test this hypothesis, we shall propose a series of numerical experiments where the importance of these three parameters is systematically explored. Except for the boundary forcing to the east, we shall investigate this problem with a simple adiabatic primitive equation model capable of describing the beta effect and the influence of bottom topography.

3. Lateral boundary forcing at 75°E

An important ingredient of our present study is the prescription of lateral boundary conditions at 75°E. We feel that this forcing is crucial for the simulation of the low-level jet. This lateral forcing is essentially derived from a study of a numerical simulation of the broad-scale monsoons carried out by Murakami *et al.* (1970). Because of the importance of this for our study, and also because of its relevance to the basic dynamics of the broadscale monsoons, we shall present a short review of this work here.

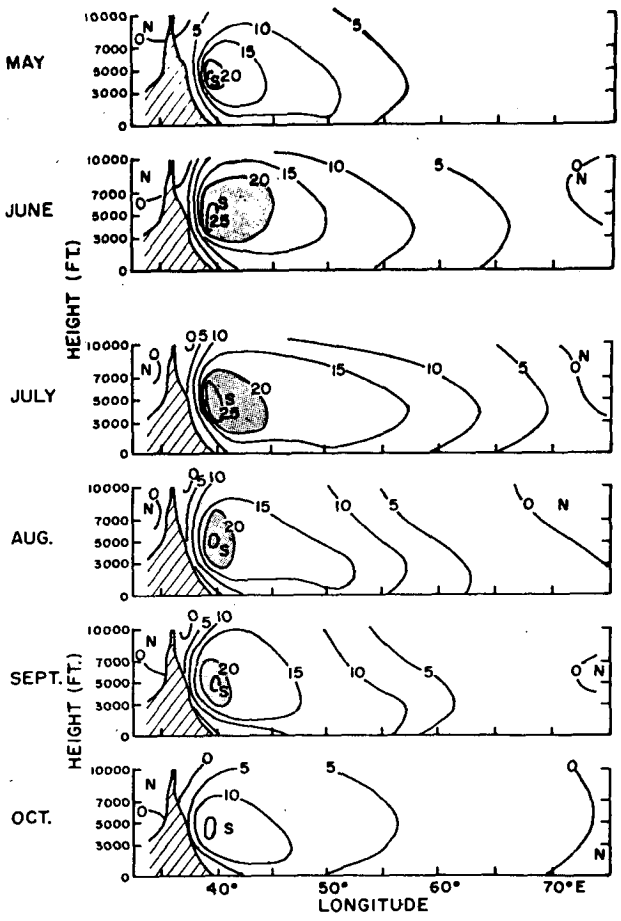

FIG. 2. Zonal vertical cross section of monthly mean meridional wind speed near the equator, following Findlater (1971). Areas larger than 20 kt are stippled. The Kenya highlands are the mountains illustrated here.

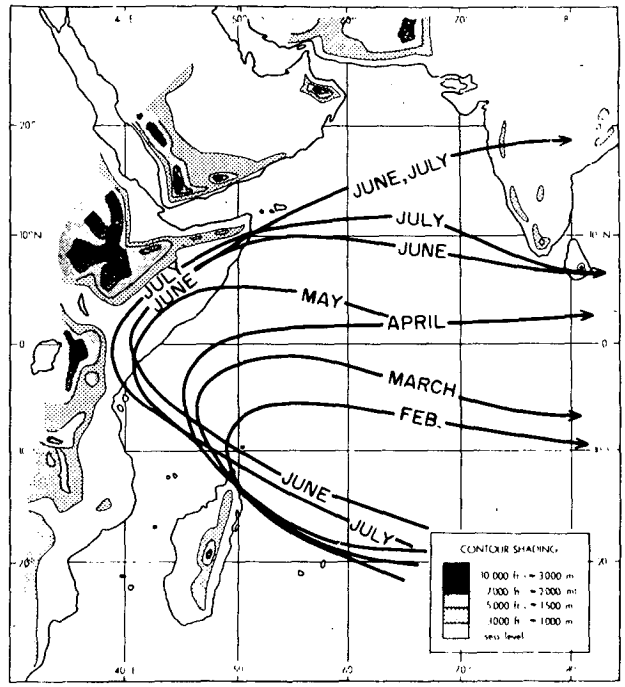

FIG. 3. Month-by-month progression of the axis of the low-level jet at the 1 km level following Findlater (1971).

a. *A review of the theory of broad-scale monsoons*

The theory is based on the solution of a zonally symmetric detailed model based on the primitive equations. In the following we shall present the closed system of equations used by Murakami *et al.* (1970). A list of symbols appears in Table 1. They adopted the zonally symmetric version of the more complete equations originally proposed by Smagorinsky *et al.* (1965) for a general circulation model.

INDEPENDENT VARIABLES: ϕ (latitude), $\sigma=P/p^*$ vertical coordinate (where p is pressure and p^* is station level pressure) and time t.

DEPENDENT VARIABLES: Zonal velocity u, meridional velocity v, vertical velocity $d\sigma/dt$ (and $\omega=dp/dt$), temperature T, mixing ratio r, surface pressure p^* and geopotential height of a σ surface Φ.

The following is their closed system of equations:

Zonal equation of motion

$$\frac{\partial}{\partial t}p_*u=-\frac{\partial p_*uv\cos\phi}{a\cos\phi\partial\phi}-\frac{\partial p_*u\sigma^0}{\partial\sigma}+\left(f+\frac{\tan\phi}{a}u\right)v+p_*F_\lambda. \quad (1)$$

Meridional equation of motion

$$\frac{\partial}{\partial t}p_*v=-\frac{\partial p_*v^2\cos\phi}{a\cos\phi\partial\phi}-\frac{\partial p_*v\sigma^0}{\partial\sigma}-\left(f+\frac{\tan\phi}{a}u\right)u$$
$$+\sigma\frac{\partial\phi}{\partial\sigma}\frac{\partial p_*}{a\partial\phi}-p_*\frac{\partial\Phi}{a\partial\phi}+p_*F_\phi. \quad (2)$$

Hydrostatic law

$$\frac{\partial\Phi}{\partial\sigma}=-\frac{RT}{\sigma}. \quad (3)$$

First law of thermodynamics

$$\frac{\partial p_*T}{\partial t}=-\frac{\partial p_*Tv\cos\phi}{a\cos\phi\partial\phi}-\frac{\partial p_*T\sigma^0}{\partial\sigma}-\frac{\omega}{c_p}p_*\sigma^0+p_*F_T. \quad (4)$$

Moisture conservation law

$$\frac{\partial p_*r}{\partial t}=-\frac{\partial p_*rv\cos\phi}{a\cos\phi\partial\phi}-\frac{\partial p_*r\sigma^0}{\partial\sigma}-p_*C+p_*F_r. \quad (5)$$

Mass continuity equation

$$\frac{\partial p_*}{\partial t}=-\frac{\partial p_*v\cos\phi}{a\cos\phi\partial\phi}-\frac{\partial p_*\sigma^0}{\partial\sigma}. \quad (6)$$

Vertical velocity equation

$$\omega=p_*\sigma^0+\sigma\left(\frac{\partial p_*}{\partial t}+v\frac{\partial p_*}{a\partial\phi}\right). \quad (7)$$

The above closed system of equations contains a number of source-sink terms for momentum, heat and moisture.

In the momentum equation F_λ and F_ϕ are frictional effects in the zonal and meridional directions. These are expressed in terms of surface stresses for the $\sigma=1$ surface and in terms of diffusive terms above a surface Prandtl layer. F_T and F_r are diffusive terms in the thermal and moisture equations. They describe both lateral and vertical mixing processes. The land and ocean areas are differentiated by the use of slightly different surface drag coefficients. Bulk aerodynamic formulas are used for the transfer of momentum, moisture and sensible heat from the lower boundary.

Other physical effects included in this model are as follows:

1) Detailed radiative heating calculation, consisting of (a) shortwave radiative warming of the atmosphere at any level and the earth's surface, (b) longwave radiative warming (or cooling) of the atmosphere at any level and the earth's surface, and (c) heat balance of the earth's surface, including sensible and latent heat fluxes at the air-sea interface.

2) Dry convection, invoked via dry convective adjustment, following Manabe *et al.* (1965).

TABLE 1. List of useful symbols.

Symbol	Meaning
x, y, p, t	independent variables, pressure a vertical coordinate
u	zonal velocity
v	meridional velocity
ω	vertical velocity $[=dp/dt]$
p^*	station-level pressure
σ	p/p^*
σ^0	$d\sigma/dt$
Φ	geopotential height of a σ surface
z	height of free surface above mountains
h	height of mountains above sea level
T	temperature
r	mixing ratio of water vapor
ϕ	latitude
a	radius of earth
f	Coriolis parameter
β	beta parameter
R	gas constant for dry air
c_p	specific heat at constant pressure
g	acceleration of gravity
F_λ	frictional force per unit mass of air in the zonal direction
F_ϕ	frictional force per unit mass of air in the meridional direction
F_T	thermal diffusion in the meridional direction
F_r	moisture diffusion
C	condensation per unit mass of air
ζ_p	potential vorticity
E_T	total energy
k	kinetic energy per unit mass
ψ	streamfunction

3) Moist convection, invoked via moist convective adjustment, following Manabe *et al.* (1965).

4) Large-scale condensation following Smagorinsky *et al.* (1965).

5) The mountains are the lower boundary of the sigma frame of coordinates. Smoothed mountains include the Himalayas with a maximum height of roughly 3000 m.

It should be noted that *the heat balance of the earth's surface is a crucial element in the dynamics* of the zonally symmetric monsoons. The soil temperature over the land area is determined from the following components of the energy exchange at the earth's surface:

Incoming and reflected shortwave radiation.
Incoming longwave radiation.
Outgoing longwave radiation.
Sensible heat flux.
Latent heat flux.

The solar zenith angle is kept at mean July daytime position. The effects of variable cloud cover are not included in the estimation of short and longwave radiation. A number of empirical parameters enter this calculation:

(i) Albedo of the surface (based on Smithsonian Tables, 1958).

(ii) Surface ground wetness (Manabe *et al.*, 1965).
(iii) Absorption and Emissivity Tables based on Manabe and Möller (1961).
(iv) Surface roughness (Manabe *et al.*, 1965).
(v) Climatological cloud cover.
(vi) Vertical distribution of ozone and carbon dioxide (Ramanathan and Kulkarni, 1960; Murgatroyd, 1964).

The lower boundary is assumed to be ocean south of 15°N, land from 15° to 80°N and ocean north of 80°N. The ocean temperatures are kept fixed during the integration.

There are eight vertical layers in the model. Finite differencing schemes consist of the semimomentum form for advection following Shuman (1960) and centered differencing in time, with an occasional forward difference to control the time-splitting of solutions.

Originally the model was integrated from the equator to the North Pole and since has been run at Florida State University from 35°S to the North Pole.

b. Results

Here we present a very brief review of the Murakami *et al.* (1970) integration that yielded the best results. All of the above-mentioned physical features including mountains were incorporated. The model starts from a state of rest with an initial temperature and moisture stratification which is a local standard atmosphere. The heat balance condition warms the soil and large fluxes of sensible heat, as well as latent heat, are produced. The surface temperature of the soil reaches near 60°C under the conditions of the fixed zenith angle of the sun. In the very lowest layer, the warming of the air results in dry static instability which is removed via dry convective adjustment. Conditional instability is removed by the moist convective adjustment process. As a result of the dry and moist convective adjustment, the upper troposphere slowly warms, pressure lowers near the surface, and high pressure forms in the upper troposphere over the land area. This manifests itself in a build-up of the available potential energy in the north-south plane. As a consequence of the lowering of the pressure, frictional convergence of mass and moist air occurs in the lower layer. This mass circulation represents a slow formation of Hadley-type vertical circulation, with ascending motions over the land areas and descent over the southern oceans. This process of warm air rising and relatively cold air sinking is shown to generate kinetic energy of the mean meridional circulation from the available potential energy in the model. The scale of the large-scale meridional overturning is about 30° latitude. In this sense, the process thus far is akin to a giant sea breeze. However, due to the large scale of the overturning, easterly zonal flows intensify in the upper troposphere and manifest themselves as an easterly jet. At lower levels southwest flows form. The energetics of the Murakami *et al.* broad-scale monsoons are schematically illustrated in Fig. 4. Zonal symmetry evidently is a major drawback of this theory. The entire broad-scale monsoons are driven by meridional differential heating. In the statistical steady state all of the energy received by zonal motions must be dissipated by frictional effects. There is no mechanism for gain or loss of kinetic energy from other horizontal scales of motion in this symmetric frame.

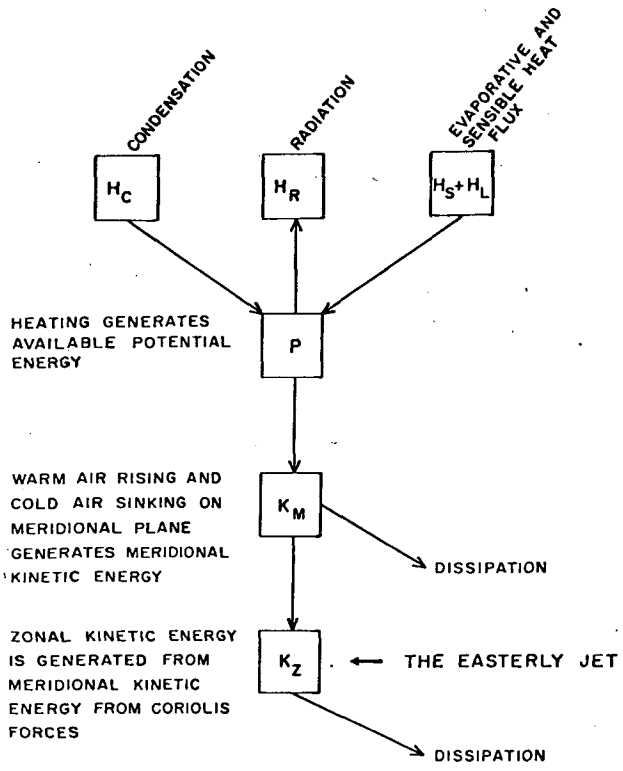

FIG. 4. The energy flow directions in the numerical simulation of the broad-scale monsoons following Murakami *et al.* (1970).

In Fig. 5a and 5b we show a comparison of the Murakami *et al.* simulation of the zonal flows on day 80, with a typical observed vertical cross section. The broad-scale features, although perhaps somewhat displaced in latitude, are extremely well simulated. Other features, not shown here, such as tropospheric temperature and moisture structure, pressure and vertical circulation all seemed reasonable compared to what is presently known from observations.

At low levels they find southerly flows ($v>0$) and easterlies ($u<0$) south of the equator and westerlies ($u>0$) north of the equator. In this sense this zonally symmetric model does simulate the southeast trades of the Southern Hemisphere and the southwest monsoons of the Northern Hemisphere. It is this geometry of the low-level flows (at 1.5 km) that we shall use as a broad-scale forcing for the region to the west of 75°E.

This solution can thus act as a forcing for the domain

to its west over the Arabian Sea and east Africa. Murakami *et al.* (1970) also present several other controlled experiments.

4. Numerical model for the simulation of the Somali jet

Here we shall describe the basic one-level primitive equation model which is utilized to test the hypothesis stated in Section 2.

a. Basic equations

Zonal equation of motion

$$\frac{\partial u}{\partial t}+u\frac{\partial u}{\partial x}+v\frac{\partial u}{\partial y}=+fv-g\frac{\partial z}{\partial x}-g\frac{\partial h}{\partial x}. \tag{8}$$

Meridional equation of motion

$$\frac{\partial v}{\partial t}+u\frac{\partial v}{\partial x}+v\frac{\partial v}{\partial y}=-fu-g\frac{\partial z}{\partial y}-g\frac{\partial h}{\partial y}. \tag{9}$$

Mass continuity equation

$$\frac{\partial z}{\partial t}+u\frac{\partial z}{\partial x}+v\frac{\partial z}{\partial y}=-z\left(\frac{\partial u}{\partial x}+\frac{\partial v}{\partial y}\right). \tag{10}$$

These are the shallow-water equations with bottom topography. The mountain height is h and the free-surface height is $z+h$. The Coriolis parameter f is defined via an equatorial beta-plane assumption.

Over a closed region, the area-mean values of

$$\text{energy } E_T=z(k+\tfrac{1}{2}gz+gh), \tag{11}$$

$$\text{potential vorticity } \zeta_p=z^{-1}\left(\frac{\partial v}{\partial x}-\frac{\partial u}{\partial y}+f\right), \tag{12}$$

are conserved. The mean potential vorticity and mean-square potential vorticity are conserved in a mechanically closed region because they are conserved following a parcel and no parcels leave the region.

b. Boundary conditions

On all boundaries u, v and z are constant with time. On all but the east boundary $u=v=0$ (in Section 3 we have discussed the boundary conditions to the east). On the north and south boundaries, z is kept equal to a constant (1.5 km). The height of the free surface on the east and west boundaries is determined by an initialization procedure.

c. Initialization procedure

In order to start the simulation experiment, u, v and z must be known. As stated earlier, $u=v=0$ at all interior points. The initial z field was determined by the following procedure:

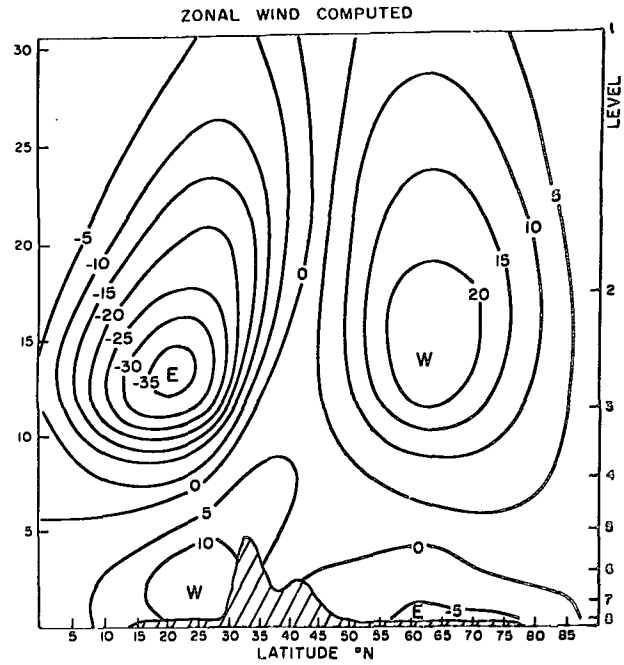

FIG. 5a. Meridional cross section of zonal velocity (m s^{-1}) on day 80 from the Murakami *et al.* (1970) numerical simulation of zonally symmetric monsoons.

1) Adjust the u component of the wind on the east boundary to make the net mass flux equal to zero. The adjusted u component is defined by

$$u_a=u-\epsilon|u|, \tag{13}$$

where

$$\epsilon=\frac{\sum_j u_j\Delta y}{\sum_j|u_j|\Delta y}. \tag{14}$$

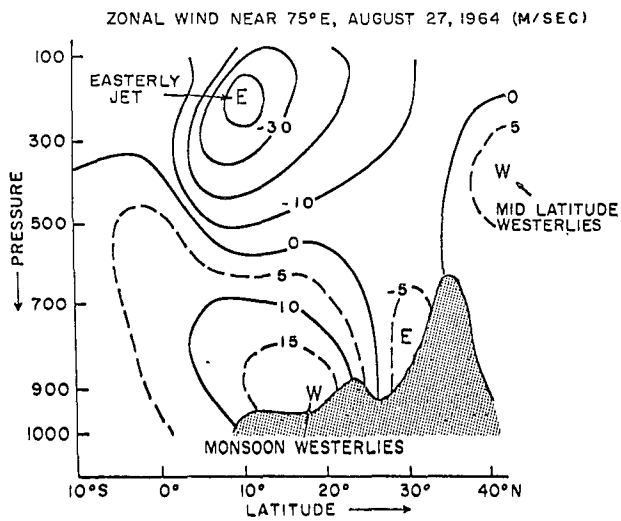

FIG. 5b. Typical observed meridional cross section of zonal velocity (m s^{-1}) near 75°E during the summer monsoon season.

2) Calculate a streamfunction ψ on the east boundary by using

$$\left.\begin{aligned}\psi_{j=1}&=0\\ \psi_{j+1}&=\psi_j-u_{j+1}\Delta y\end{aligned}\right\}. \tag{15}$$

3) Set the streamfunction at the adjacent column to half its value on the east boundary. At all other points the streamfunction is set to zero.

4) Compute the geopotential height $(z+h)$ from the streamfunction using the nonlinear balance equation, following Krishnamurti (1969).

The initial geopotential field is relatively flat except near the east boundary.

d. Finite-difference scheme for prediction

Eqs. (8), (9) and (10) are integrated by a semi-Lagrangian advective scheme following Mathur (1970) and Krishnamurti (1969). This scheme is modified to prevent a separation of solutions in space due to centered differencing of the horizontal derivative terms. This is accomplished by following a procedure suggested by Kanamitsu (1975). It entails a reduction of truncation error by calculating higher order corrections for the pressure gradient force and incorporating its effect on the divergence term in the mass continuity equation. The time-differencing scheme along the short semi-Lagrangian parcel paths is the well-known Euler backward scheme discussed by Krishnamurti (1969). The integration is carried out over a 1° latitude/longitude mesh of 2601 grid points.

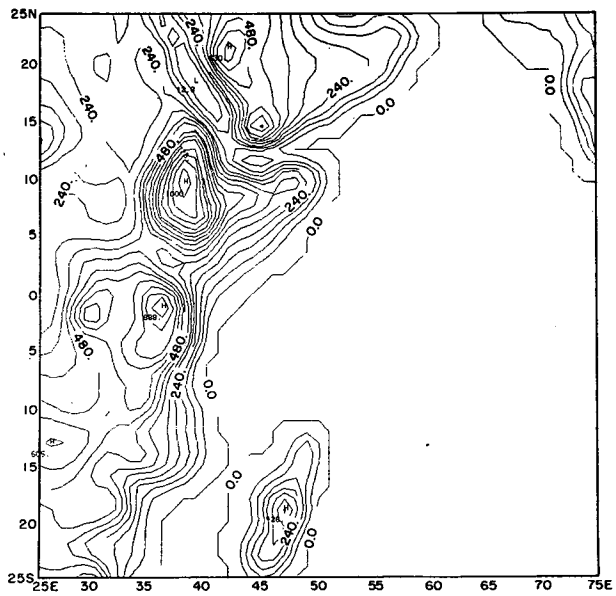

FIG. 6. Terrain height (m) over the domain of the study. The heights shown here are based on Gates and Nelson (1975).

e. Smoothed topography

Fig. 6 shows the mountain heights used in this study. The heights were obtained from the recent tabulations of Gates and Nelson (1975). The heights were linearly interpolated to the latitude/longitude grid and smoothed with a standard nine-point smoother. In addition, the maximum height of the mountains was suppressed to 1 km using the relation

$$h_{\text{modified}}=h_{\text{original}}\times 1000/h_{\max}, \tag{16}$$

where $h_{\max}$ is the maximum height of the smoothed terrain in our computational domain. This procedure was used because 1) the maximum slope of the modified mountain was of the order of 10^{-3} and our model was able to handle this without any computational smoothing of the pressure gradient force, and 2) we were interested in the 1.5 km level flows and we wished to explore the influence of bottom topography (especially the east African highlands) and not of a rigid side wall boundary at this stage. It should be noted that although the bottom topography is felt by the free surface flows, the flow can travel freely over the mountain ranges.

5. Results of numerical simulation of the Somali jet

Here we shall describe the results of five numerical experiments.

a. Experiment 1

In this experiment complete terrain and the beta effect are included, and the zonally symmetric monsoon forcing is included at 75°E. The results of the integration at day 6.5 are illustrated in Fig. 7. The top panel depicts the vector motion field and the lower panel the isotachs of the free surface flows. The behavior of the "invariants" of the flow during integration is shown in Table 2. Although the mass flux is zero on the east boundary, exact invariance cannot be expected because the boundary is not mechanically closed. However, a large departure from invariance would make it difficult to interpret the results. Table 2 indicates that the total energy was closely conserved and that, after rising slowly for most of the integration period, the mean and mean square potential vorticity are nearly constant during the last 12 h. In view of these results, the simulated field at day 6.5 will be discussed.

In Experiment 1 (Fig. 7), the following features of the cross-equatorial jet may be noted in the simulations:

1) The axis of the low-level jet, a heavy dark line, goes westward in the southern Indian Ocean just north of Madagascar and northward near the east African mountains and turns eastward over southern Somalia and then toward the central Arabian Sea.

2) A relative minimum in speed along the jet axis near the equator.

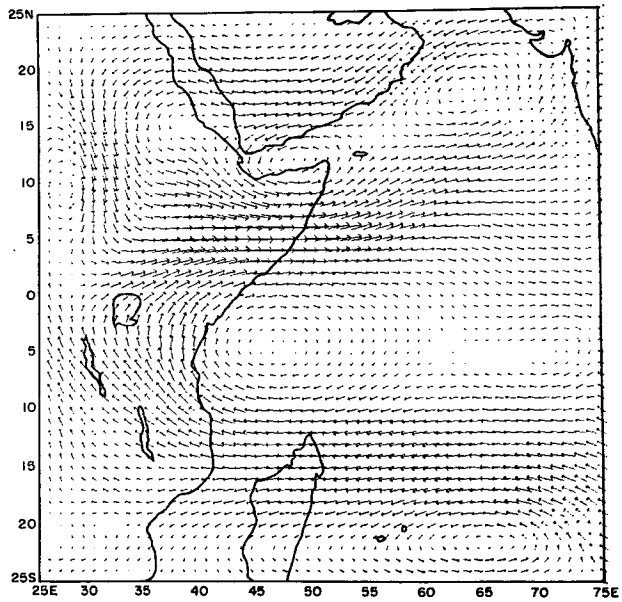

FIG. 7a. Solution of vector plots on day 6.5 for Experiment 1. This experiment includes terrain, the beta effect and a lateral broad-scale monsoon forcing.

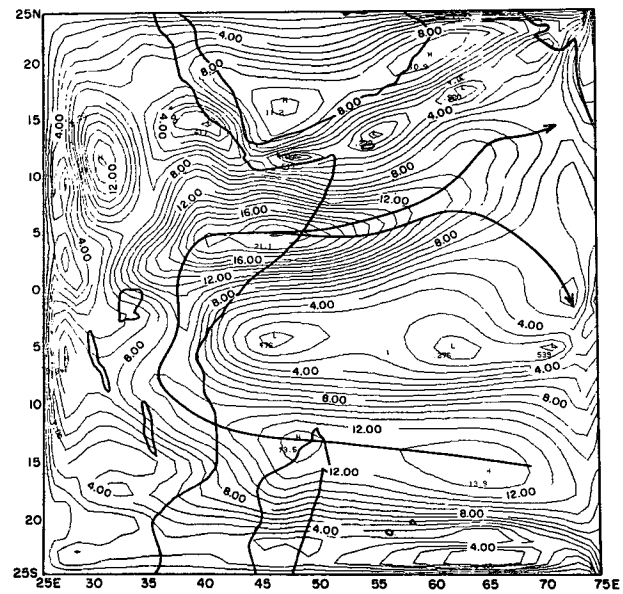

FIG. 7b. The speed field (m s^{-1}) for Experiment 1 showing the simulated features: axis of the low-level jet, strong winds near the Somali coast and downstream from Madagascar, relatively weak winds near the equator and a split of the jet axis over the Arabian Sea.

3) A strong jet off the Somali coast.
4) A speed maximum downstream from Madagascar.
5) A major split of the Somali jet over the Arabian Sea.

The maximum speed off the Somali coast on day 6.5 is of order of 25 m s^{-1} which is a reasonable speed.

TABLE 2. Domain average values for Experiment 1.

Hour	Mean height of free surface (m)	Mean potential vorticity (10^{-10} m^{-1} s^{-1})	Mean square potential vorticity (10^{-16} m^{-2} s^{-2})	Total energy (10^{6} m^{3} s^{-2})
24	1346.8	9.9	8.5	9.1
48	1344.2	10.8	9.9	9.1
72	1341.8	12.4	10.1	9.1
96	1339.9	16.5	10.3	9.0
120	1338.2	19.8	10.4	9.0
144	1337.0	21.5	10.6	9.0
156	1336.7	21.5	10.7	9.0

Near the north-south and the western boundaries a number of weak transients are present that exhibit large changes in position during the integration and are not discussed in this paper since we feel that they are not of a major consequence for this study.

Our simulation (Fig. 7) also predicts a velocity maximum near 65°E and 15°S, a region not covered by observations presently. It may be of interest to observe whether such a velocity maximum exists this far upstream from Madagascar. Surface "ships of opportunity" in this region do indicate strong surface winds, and this is also recognized as a region where large air-sea interaction occurs.

Fig. 8 shows the isopleths of potential vorticity on day 6.5 for Experiment 1. The interval is 90×10^{-10} m^{-1} s^{-1}. Because absolute vorticity is largely positive in the Northern Hemisphere and negative in the Southern

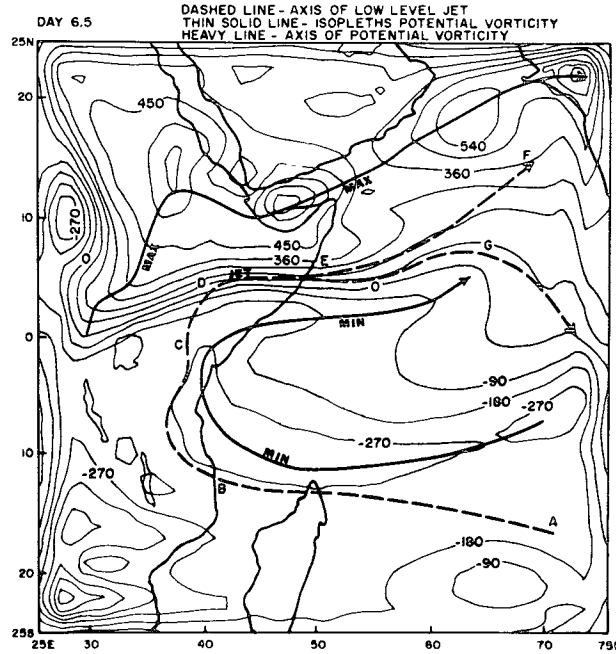

FIG. 8. Isopleths of potential vorticity (10^{-10} m^{-1} s^{-1}) for Experiment 1.

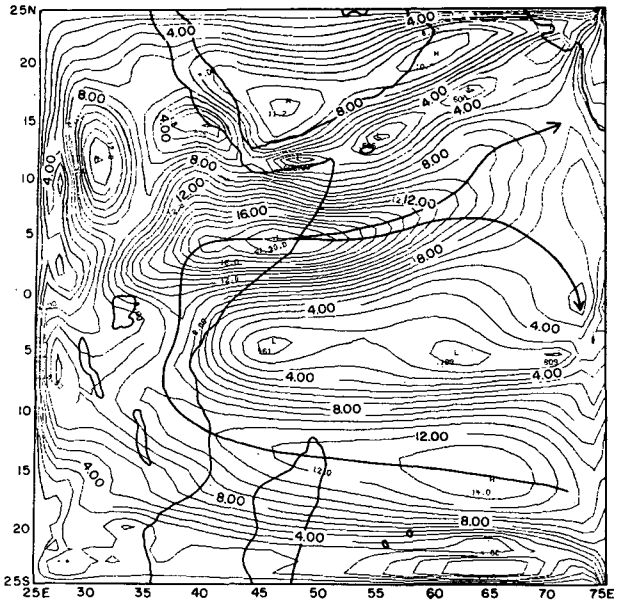

FIG. 9. Isotachs (m s^{-1}) for Experiment 2 on day 6.5. The Madagascar mountains are removed. Otherwise as in Experiment 1.

Hemisphere, the potential vorticity exhibits similar behavior. The dashed lines in Fig. 8 represent the jet axis of the free surface, and the heavy solid lines are the axes of potential vorticity maxima and minima. The jet is confined to the region between these two axes.

It should be noted that a truly steady state is not reached in this problem. Although the area-mean vorticity and mean-square vorticity are nearly constant by day 6.5, the streamlines of the flow vary slowly in time. As a result, potential vorticity is not always constant along the streamlines.

The letters A through G in Fig. 8 represent some selected points along the jet axis. The potential vorticity is nearly constant from A to B in the South Indian Ocean, and from E to G along the southern branch of the split jet in the Arabian Sea. Between C and D over east Africa the flow encounters a rapid increase in the height of the bottom topography (Fig. 6). The fluid depth decreases rapidly here, and because potential vorticity is conserved along a trajectory, the flow acquires large anticyclonic curvature. As the flow travels eastward from D to E, the height of the bottom topography decreases, and the flow acquires cyclonic curvature. The potential vorticity behavior is somewhat complex over the rest of the domain. The transient nature of the flows, especially near the west boundary, makes it difficult to interpret many of the small-scale details.

In order to see the relative importance of the various parameters such as bottom topography, beta parameter and the broad-scale monsoon forcing, we present the following additional experiments.

b. Experiment 2

The east African mountains, the beta effect, and the broad-scale monsoon forcing at the eastern boundary are included, but the Madagascar mountains are removed. The results on day 6.5 are illustrated in Fig. 9. This figure should be compared with Fig. 7 of Experiment 1. The results of simulation are nearly identical in the two experiments except for the absence of a velocity maximum just downstream from the northern tip of Madagascar. The Madagascar mountains seem to be important for a local downstream intensification of the low-level jet.

c. Experiment 3

The beta effect and the broad-scale monsoon forcing at 75°E are included; however, the entire bottom topography was suppressed. Fig. 10 illustrates the solution of the isotach field on day 6.5 for this experiment. The flows extend to the western boundary and a number of quite unrealistic gyres develop in this experiment. The entire solution is constrained by the size of the computational domain and momentum accumulates near the western wall. Strong winds are not present near the Somali coast. The key features of the observed jet are not simulated when the mountains are removed.

d. Experiment 4

In this experiment the beta parameter was set equal to zero while retaining the bottom topography and the broad-scale monsoon forcing at 75°E. Because the

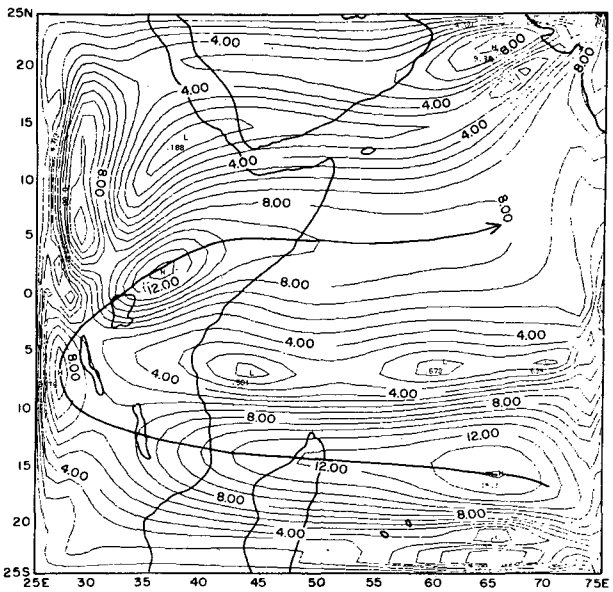

FIG. 10. Isotachs (m s^{-1}) for Experiment 3 on day 6.5. The beta effect and the lateral broad-scale monsoon forcing are included. The mountains are completely removed in this experiment.

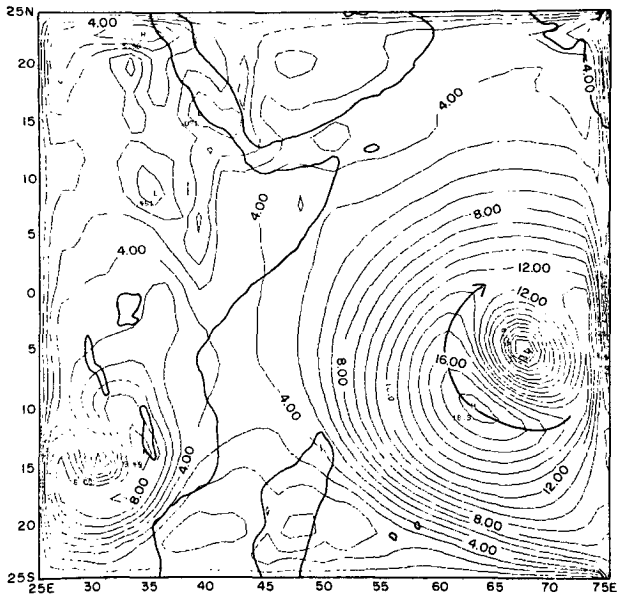

FIG. 11. Isotachs (m s^{-1}) for Experiment 4 on day 6.5. The beta effect is removed, while the mountains and the lateral broad-scale monsoon forcing are included.

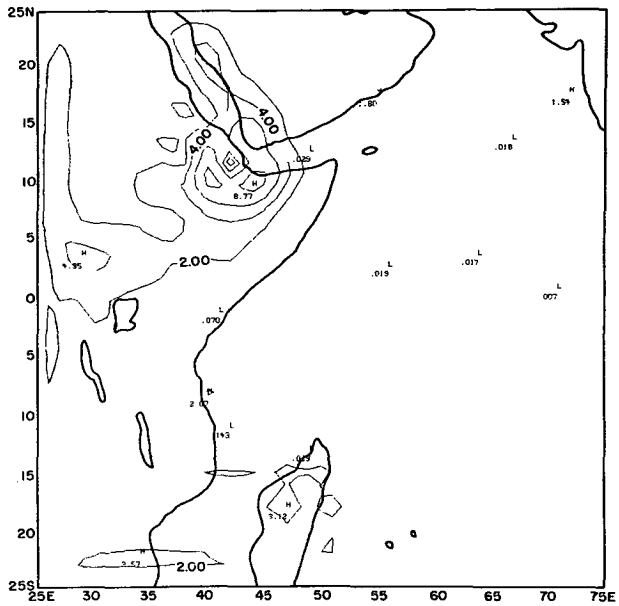

FIG. 12. Isotachs (m s^{-1}) for Experiment 5 on day 6.5. This experiment includes mountains, the beta effect and a weak lateral broad-scale monsoon forcing.

equator is the central latitude in the domain of integration, this is equivalent to setting $f=0$ everywhere as well. The solution of the isotach field on day 6.5 is illustrated in Fig. 11. This solution shows almost no resemblance to observations. It is thus quite clear that the beta parameter is very important for the simulation of the Somali jet.

e. Experiment 5

This experiment includes the complete bottom topography and the beta effect. However, the broad-scale monsoon forcing at 75°E was reduced by a factor of 10 from the other experiments. This experiment never develops any semblance to the observed flows, even after 10 days of integration. Fig. 12 shows the solution after 6.5 days. This experiment illustrates the importance of the broadscale forcing to the east for the realistic simulation of the Somali jet. This implies that if the broad-scale monsoon forcing is weak, then the cross-equatorial low-level jet may also be weak. If this is true, it may have important implications for the monsoon problem.

There is observational evidence to suggest that there does exist some relationship between central India rainfall and the Somali jet. Fig. 13 illustrates central India rainfall for the drought year 1972 compared with near-normal rainfall during 1973 (the envelope is the daily normal rainfall value). The 850 mb winds during these two years for Mogadiscio, Somalia are illustrated in the same diagram. This suggests that during the drought year (when the broad-scale forcing at 75°E was weak), the seasonal mean Somali jet was also weak.

Findlater (1969a) has alluded to some relationships between the monsoon rainfall over western India and the strength of the cross-equatorial low-level jet over

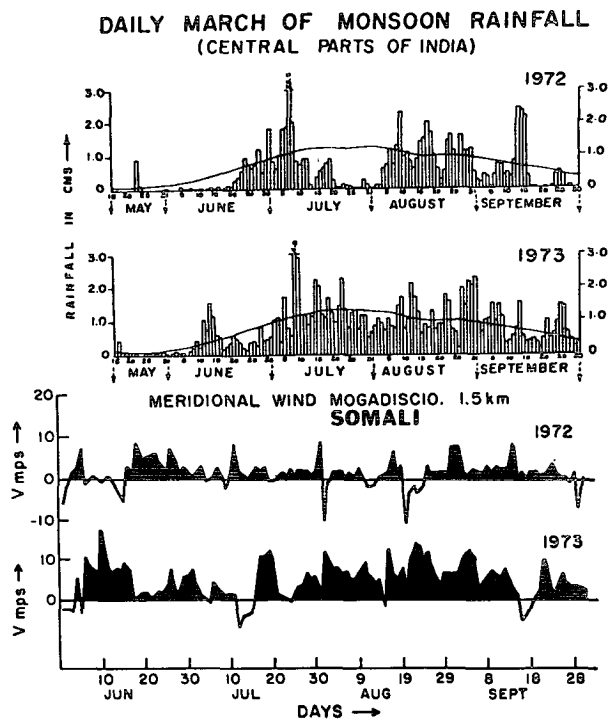

FIG. 13. (Top) daily rainfall (cm) over central India for 1972 (drought year) and 1973 (normal rainfall year). The daily long-term normal rainfall is shown by the envelope line. (Bottom) daily winds at 1.5 km over Somalia for the years 1972 and 1973. Note that during 1972 Somali winds are weak compared to 1973.

equatorial east Africa. He found a lag in this problem where the strong winds at Garissa in Kenya precede rainfall maxima over western India by a few days. What we are presenting here is somewhat of an inverse story for the broad-scale forcing and its response—the response being the cross-equatorial low-level jet. With a strong forcing at 75°E, we obtain a strong jet (Fig. 7), and with a weak forcing we find only weak flows over east Africa. This problem is discussed further in Section 7.

f. On the splitting of the Somali jet

The splitting of the Somali jet into two main branches in the central Arabian Sea is an important question. Observations and our simulations do exhibit a split of the Somali jet. In order to explore this question, we examined barotropic instability as a possible mechanism for this phenomenon. Splitting of jets as a barotropic phenomenon has been mentioned in several studies (Thompson, 1957; Arakawa, 1961; Wiin-Nielsen, 1961; and others). The basic idea here would be that the flows near the Somali coast become so strong that large divergence of flux of westerly momentum would occur near the principal jet. As a consequence, there would be other regions with a large net convergence of flux of westerly momentum. The parent jet would weaken as a consequence of the divergence of flux and a new jet would form somewhere in its vicinity due to the convergence of flux of momentum. A split jet phenomenon may be observed when such a mechanism is operating. Arakawa (1961) presents a very interesting illustration of this mechanism in a simple climatic-type barotropic closure problem.

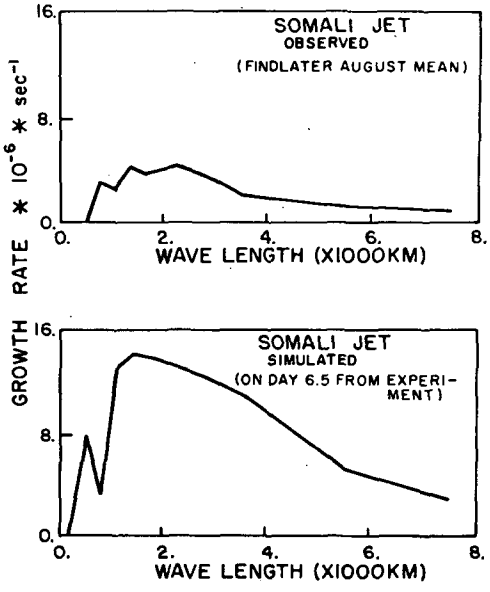

FIG. 14. Barotropic instability diagrams for the observed and the simulated Somali jet near 45°E. The growth rate is illustrated as a function of horizontal scale.

TABLE 3. Convergence and divergence of flux of momentum for the split jet at 75°E.

Latitude	Speed ($m\ s^{-1}$)	Divergence of flux of momentum ($10^{-5}\ m\ s^{-2}$)
5°S	1.0	0.9
4°	2.9	1.0
3°	4.2	0.1
2°	5.0	−0.9
1°	5.4	−1.5
0°	5.5	−1.4
1°N	5.4	−1.1
2°	5.4	−0.8
3°	5.4	−0.5
4°	5.4	−0.1
5°	5.4	0.4
6°	5.5	1.2
7°	5.7	2.1
8°	5.8	2.9
9°	5.9	3.3
10°	6.1	3.9
11°	6.6	4.5
12°	7.0	4.2
13°	7.1	2.5
14°	7.0	0.1
15°	6.7	−1.9

We performed a calculation of the barotropic instability by the so-called finite-difference method for determining the unstable scales following Haltiner (1963) and Yanai and Nitta (1968). This method is illustrated in the Appendix. The flows of the observed, as well as the simulated, Somali jet near the Somali coast close to 45°E were subjected to this analysis. The results are portrayed in a stability diagram showing a plot of growth rate versus horizontal scale (Fig. 14). We interpret the results of the most unstable wave around 2000 km as follows. The influence of the Ethiopian highlands, east African highlands, and inertial effects is to produce a very intense low-level jet near the Somali coast. The profile of absolute vorticity satisfies the necessary condition for the existence of barotropic instability. We further note that the northern branch of the jet experiences a divergence of flux of westerly momentum at 70°E (Table 3), while the southerly branch is located in a region of convergence of flux. These distributions of the convergence and divergence of flux of westerly momentum are consistent with the notion of barotropic instability. The southern part of the split jet does have a wave-like structure along its axis, and the wavelength seems close to 2000 km.

In Fig. 14 the scale of the most unstable wave for the observed monthly mean jet is slightly longer than that for the simulated jet. This is not surprising considering that the monthly mean jet of Findlater is comparatively broader and weaker than the simulated jet.

6. Limitations of present work

A number of other physical effects evidently are important for the detailed definition of the low-level jet that are not included here. Some such factors are as follows:

- Air-sea interaction over the Arabian Sea and Indian Ocean. The upwelling and associated cold coastal waters of western oceans must have an important influence on the precise definition of the jet.
- Over the land mass of Arabia, the low-level summer northerlies are not simulated properly here, since the adiabatic physics is not adequate for this problem. A detailed three-dimensional model with the heat balance of the earth's surface over the Arabian deserts would be necessary. Hahn and Manabe (1975) and Washington and Daggupaty (1975) include this physics in their general circulation model, which describes the monsoons.
- Influence of shallow and deep convection is not included in our study.
- The vertical structure of the jet is not considered here. The explanation for why the jet is confined to levels below 700 mb and why it has vertical shears on the order of 30 m s^{-1} Km^{-1} is beyond the scope of this study.
- The influence of a detailed boundary layer dynamics is not present in our study.
- Large-scale ascending and descending motions of the broad-scale monsoon system over the Arabian Sea are not present.
- Presently we only have provision for a one-way interaction of the happenings over the Indian Ocean-Arabian Sea region with the lateral boundary over India. In our study the latter is defined and fixed from the Murakami *et al.* (1970) simulations of the zonally symmetric monsoons. In nature, transients can form in the low-level jet due to factors such as inertial and barotropic instabilities; such instabilities could enhance local wind maxima and modify local air-sea interactions. These, in turn, can modify the nature of the broad-scale monsoons over India. For the present, we do not consider this feedback of transients into the broad-scale monsoons. However, it should be noted that transients do exist within our computational domain.

The limitations stated above could be handled by a multi-level detailed model. Our intention here is to present a "minimal system" that is capable of simulating the horizontal concentration of momentum in the low-level jet in approximately the correct geographical locations.

7. Concluding remarks

Further refinements of the present simulation can be accomplished by introducing more physics and better treatment of the mountains. This study has outlined the major importance of the east African-Madagascar mountains, the beta effect and the broad-scale monsoon forcing over India for the dynamics of the Somali jet.

We feel that the broad-scale low-level jet is forced by the differential land-ocean contrast heating over India. There are evidently many kinds of transients in the monsoon dynamics problem. By prescribing the forcing at 75°E we do not permit a feedback of the transients in the low-level jet to modify the monsoons at 75°E. The kind of 2–3 day response of the monsoons over India to the transients in the low-level jet was addressed by Findlater. A more complete model would be required to examine the mutual interaction problem. We feel that the direction of the feedback may be dependent on scales, the larger scale response going from India to East Africa while the shorter scale responses may be of the opposite nature.

The observational aspects of the low-level jet presented here rely heavily on Findlater's work. As may be seen from Fig. 1, there are many data-void regions in the Arabian Sea and the Indian Ocean. This deficiency will hopefully be somewhat corrected during the forthcoming GARP Monsoon Experiment which is scheduled for the year 1979.

Acknowledgments. This work was supported by the National Science Foundation under Grant ATM75-18945. Computations were carried out on Florida State University's CDC 6400 and on the CDC 6600/7600 system of the National Center for Atmospheric Research which is sponsored by the National Science Foundation.

APPENDIX A

Finite-Difference Method of Finding Barotropic Instability

Here we present a brief review of the finite difference method following Haltiner (1963) and Yanai and Nitta (1968). Our analysis is carried out at 45°E for both the observed (Fig. 1) and simulated (Fig. 7) zonal flows.

HALTINER, YANAI-NITTA METHOD

The linearized barotropic vorticity equation is the starting point of this analysis. We start from the barotropic nondivergent vorticity equation

$$\frac{\partial}{\partial t}\nabla^2\psi = -\mathbf{V}_H\cdot\nabla(\nabla^2\psi) - \beta\frac{\partial\psi}{\partial x}, \tag{A1}$$

where $\mathbf{V}_H = \mathbf{k}\times\nabla\psi$ and ψ is the streamfunction. If a basic zonal flow is defined by $\bar{u} = -(\partial\bar{\psi}/\partial y)$ and a perturbation streamfunction ψ' is defined by the relation $\psi = \bar{\psi} + \psi'$, the linearized barotropic vorticity equation is expressed by

$$\left(\frac{\partial}{\partial t} + \bar{u}\frac{\partial}{\partial x}\right)\nabla^2\psi' + \left(\beta - \frac{d^2\bar{u}}{dy^2}\right)\frac{\partial\psi'}{\partial x} = 0. \tag{A2}$$

Assuming a solution of the form

$$\psi'(x,y,t)=\Psi(y)e^{i\mu(x-ct)}, \tag{A3}$$

we obtain the relation

$$(\bar{u}-c)\left(\frac{d^2\Psi}{dy^2}-\mu^2\Psi\right)+\left(\beta-\frac{d^2\bar{u}}{dy^2}\right)\Psi=0, \tag{A4}$$

where μ is a wavenumber and c is a complex phase speed. The amplitude function Ψ and the phase speed c are the unknowns of the eigenvalue problem.

The finite-difference method consists of rewriting the above equation (A4) in a finite meridional domain bounded by $y=\pm d$, where $2d$ is the width of the domain over which $\bar{u}(y)$ is defined. The amplitude function Ψ is assumed to vanish at these boundaries of the domain.

Eq. (A4) is expressed in finite-difference form along the meridional coordinate using a number of evenly spaced points, $j=1, 2, \ldots, M$ at distances Δy apart from each other. The boundaries are at $J=1$ and $J=M$ where the perturbation streamfunction vanishes. (In our study $M=41$).

The resulting equation

$$(u_J-c)[(\Psi_{J+1}+\Psi_{J-1}-2\Psi_J)/\Delta y^2-\mu^2\Psi_J] +[\beta-(\bar{u}_{J+1}+\bar{u}_{J-1}-2\bar{u}_J)/\Delta y^2]\Psi_J=0 \tag{A5}$$

is homogeneous in Ψ_J and can be expressed in matrix form (Haltiner, 1963)

$$(\mathbf{B}-C\mathbf{D})\mathbf{A}=0, \tag{A6}$$

where C is the complex phase speed, $\mathbf{B}$ and $\mathbf{D}$ are square matrices involving the velocity, grid distance and the β parameter. $\mathbf{A}$ is a column vector involving the amplitudes Ψ. The necessary and sufficient condition for the existence of nonzero solutions for the amplitude function Ψ is that the matrix $(\mathbf{B}-C\mathbf{D})$ be singular. This condition may be expressed by the singularity of the matrix $(\mathbf{B}\mathbf{D}^{-1}-C\mathbf{I})$, where $\mathbf{I}$ is the identity matrix.

The complex phase velocities are the eigenvalues of the matrix $\mathbf{B}\mathbf{D}^{-1}$. From the tabulation of the growth rates for each value of C, one can determine the disturbance of the largest growth rate. Its eigenstructure can also be portrayed, as illustrated by Nitta and Yanai (1969).

REFERENCES

Arakawa, A., 1961: The variation of general circulation in the barotropic atmosphere. *J. Meteor. Soc. Japan*, **39**, 49–58.

Bunker, A. F., 1965: Interaction of the summer monsoon air with the Arabian Sea. *Proc. Symp. International Indian Ocean Expedition*, WMO., Geneva, 3–16.

Findlater, J., 1969a: A major low-level air current near the Indian Ocean during the northern summer. *Quart. J. Roy. Meteor. Soc.*, **95**, 362–380.

——, 1969b: Interhemispheric transport of air in the lower troposphere over the western Indian Ocean. *Quart. J. Roy. Meteor. Soc.*, **95**, 400–403.

——, 1971: Mean monthly air flow at low levels over the western Indian Ocean. *Geophys. Mem.*, No. 115, HMSO, London, 53 pp.

Gates, L. W., and A. B. Nelson, 1975: A new (revised) tabulation of the Scripps topography on a 1° global grid. Part I: Terrain heights. Rep. R-1276-1-ARPA. The Rand Corporation, Santa Monica, Calif.

Hahn, D. G., and S. Manabe, 1975: The role of mountains in the South Asian monsoon circulation. *J. Atmos. Sci.*, **32**, 1515–1541.

Haltiner, G. J., 1963: Finite difference approximations for the determination of dynamic stability. *Tellus*, **15**, 230–240.

Kanamitsu, M., 1975: On numerical prediction over a global tropical belt. Rep. No. 75-1, Dept. of Meteorology, Florida State University, Tallahassee. 282 pp. [Available from University Microfilms.]

Krishnamurti, T. N., 1969: An experiment in numerical prediction in equatorial latitudes. *Quart. J. Roy. Meteor. Soc.*, **95**, 594–620.

——, and H. N. Bhalme, 1976: The oscillations of the monsoon system. Part I. Observational aspects. *J. Atmos. Sci.*, **33**, 1937–1954.

Lighthill, M. J., 1969: Dynamic response of the Indian Ocean to onset of the southwest monsoon. *Phil. Trans. Roy. Soc. London*, **265A**, 45–92.

Manabe, S., and F. Möller, 1961: On the radiative equilibrium and heat balance of the atmosphere. *Mon. Wea. Rev.*, **89**, 503–532.

——, J. Smagorinsky and R. F. Strickler, 1965: Simulated climatology of a general circulation model with a hydrologic cycle. *Mon. Wea. Rev.*, **93**, 769–798.

Mathur, M. B., 1970: A note on an improved quasi-Lagrangian advective scheme for primitive equations. *Mon. Wea. Rev.*, **98**, 214–219.

Murakami, T., R. Godbole and R. R. Kelkar, 1970: Numerical simulation of the monsoons along 80°E. *Proc. Conf. Summer Monsoon of Southeast Asia*, Navy Wea. Res. Fac., Norfolk, Va., 39–51. [Available from Environmental Prediction Research Facility, Naval Postgraduate School, Monterey, Calif.]

Murgatroyd, R. J., 1964: Ozone and water vapour in the upper troposphere and lower stratosphere. WMO Tech. Note 68, No. 169 T.P. 83, pp. 68–69.

Nitta, T., and M. Yanai, 1969: A note on barotropic instability of the tropical easterly current. *J. Meteor. Soc. Japan*, **47**, 183–197.

Ramanathan, K. R., and R. N. Kulkarni, 1960: Mean meridional distributions of ozone in different seasons calculated from Umkehr observations and probable vertical transport mechanism. *Quart. J. Roy. Meteor. Soc.*, **86**, 144–155.

Shuman, F., 1960: Numerical experiments with the primitive equations. *Proc. Symp. Numerical Weather Prediction*, Tokyo, Meteor. Soc. Japan, 656 pp. [Available from World Meteorological Organization, Geneva.]

Smagorinsky, J., S. Manabe and J. L. Holloway, Jr., 1965: Numerical results from a nine-level general circulation model of the atmosphere. *Mon. Wea. Rev.*, **93**, 727–768.

Smithsonian Meteorological Tables, 1958: Smithsonian Institution, Washington, D. C.

Thompson, P. D., 1957: A heuristic theory of large-scale turbulence and long period velocity variations in barotropic flow. *Tellus*, **9**, 69–91.

Washington, W., and S. Daggupaty, 1975: Numerical simulation with the NCAR Global circulation model of the mean conditions during the Asian-African summer monsoon. *Mon. Wea. Rev.*, **103**, 105–144.

Wiin-Nielsen, A., 1961: On short and long term variations in quasi-barotropic flow. *Mon. Wea. Rev.*, **89**, 461–476.

Yanai, M., and T. Nitta, 1968: Finite difference approximations for the barotropic instability problem. *J. Meteor. Soc. Japan*, **46**, 389–403.